Title

Universal signal scaling in microwave impedance microscopy

Journal

Applied Physics Letters, 121(12)

ISSN

0003-6951

Authors

Shan, Jun-Yi

Pierce, Adam

Y., Eric

Publication Date

2022-09-19

DOI

10.1063/5.0115833

Universal signal scaling in microwave impedance microscopy

Jun-Yi Shan,[1,2] Adam Pierce,[1] and Eric Y. Ma[1,2,a)]
[1)]*Department of Physics, University of California, Berkeley, Berkeley, CA, USA*
[2)]*Lawrence Berkeley National Laboratory, Berkeley, CA, USA*

Microwave impedance microscopy (MIM) is an emerging scanning probe technique that measures the local complex dielectric function using near-field microwave. Although it has made significant impacts in diverse fields, a systematic, quantitative understanding of the signal's dependence on various important design parameters is lacking. Here we show that for a wide range of MIM implementations, given a complex tip-sample admittance change ΔY, the MIM signal – the amplified change in the reflected microwave amplitude – is $-G\cdot\Delta Y/2Y_0\cdot\eta^2\cdot V_{\text{in}}$, where η is the ratio of the microwave voltage at the probe to the incident microwave amplitude, Y_0 the system admittance, and G the total voltage gain. For linear circuits, η is determined by the circuit design and does not depend on V_{in}. We show that the maximum achievable signal for different designs scales with η^2 or η when limited by input power or sample perturbation, respectively. This universal scaling provides guidance on diverse design goals, including maximizing narrow-band signal for imaging and balancing bandwidth and signal strength for spectroscopy.

Microwave impedance microscopy (MIM) is an emerging scanning probe technique capable of non-contact measurement of local complex permittivity $\hat{\varepsilon}$ using near-field microwave[1,2]. It has been successfully applied to diverse basic and applied topics, including photo-carriers in semiconductors[3], domain walls in ferroelectric[4] and strongly-correlated materials[5], and interface states in topological systems[6,7].

While several different MIM designs have emerged over the years[8–13], most contain a microwave scanning probe with a sharp tip, an impedance matching network, and an ultrasensitive microwave reflectometer (Fig. 1). The reflectometer sends an incident microwave $V_{\text{in}}e^{i\omega t}$ to the matching network and collects the reflected signal $V_{\text{out}}e^{i\omega t}$. It often cancels the static background in V_{out} at a reference position, and then amplifies and down-converts any variations ΔV_{out} during scanning. This produces a complex signal $\Delta V_{\text{MIM}} = G\Delta V_{\text{out}}$ that is linearly proportional to variations in tip-sample admittance ΔY, which in turn result from spatial or temporal variations in $\hat{\varepsilon}$. ΔV_{MIM} can be recorded directly or processed further with, e.g., a lock-in amplifier.

Despite its wide application, a systematic, quantitative understanding of the MIM signal's dependence on the various design parameters, in particular the type of impedance matching network and the properties of the probe, is lacking. MIM images are often presented with arbitrary units, and there has been little discussion on the performance limits and signal-bandwidth trade-offs.

Here we show, numerically and analytically, a broadly-applicable relationship between the complex MIM signal and a few physically meaningful quantities:

$$\Delta V_{\text{MIM}} = -G\cdot\frac{\Delta Y}{2Y_0}\cdot\eta^2\cdot V_{\text{in}},$$

where $\eta = V_{\text{probe}}/V_{\text{in}}$ is the ratio of the microwave voltage at the probe to the complex amplitude of the incident microwave, Y_0 the system admittance, and G the total voltage gain applied to the reflected signal. For linear circuits, η is determined by the circuit design and does not depend on V_{in}.

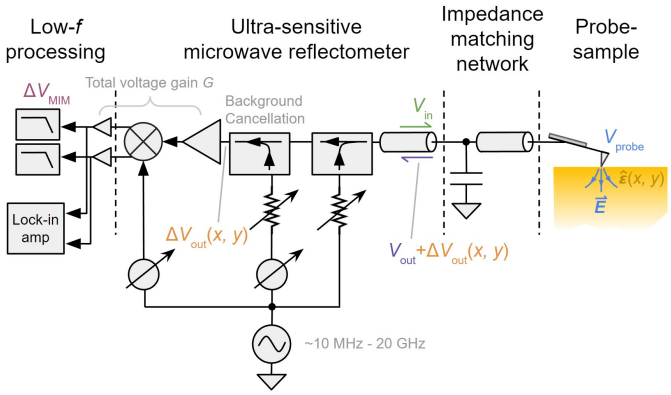

FIG. 1. Schematic of MIM. Incident microwave V_{in} is delivered to the impedance matching network and the probe via a directional coupler and a transmission line. A quasi-static voltage of V_{probe} builds up at the probe and generates microwave electric fields. The electric fields interact with the sample and translate local variations in $\hat{\varepsilon}$ into variations in the reflected microwave V_{out}. To maximize sensitivity and dynamic range, the static background in V_{out} is often canceled by a signal with identical amplitude and a π phase shift in another directional coupler. The remaining ΔV_{out} is then amplified and down-converted to near-DC by an IQ mixer, before being recorded or further processed.

This relationship applies to arbitrary impedance matching network and probe designs, at arbitrary frequencies with arbitrary impedance matching quality, as long as ΔY is small compared with the total probe impedance. We discuss its implications on the maximum signal and signal-bandwidth trade-offs in different operation limits, thus guiding new MIM designs.

First, to gain insights into how MIM signal scales with various design parameters, we simulated three distinct combinations of microwave probes and impedance matching networks: (a) a quartz tuning fork (TF) probe with half-wave matching, (b) a stripline cantilever probe with quarter-wave and stub matching, and (c) a bare metal cantilever probe with broadband shunt resistor matching (Fig. 2a-c). We assume that the probes are much smaller than the microwave wavelength so

[a)]Electronic mail: eric.y.ma@berkeley.edu

TABLE I. Simulation parameters.

Case	Probe			Impedance matching
	R (Ω)	L(nH)	C (pF)	
(a)	Bare etched W wire with tuning fork[11]: $l = 3$ mm, $d = 80$ μm			Half-wave TL: FMBC002 Fairview Microwave, $l_{\mathrm{TL}} = 57$ mm
	0.25	2.6	0.04	$C = 0.17$ pF, 0402 (R07S) S-Series Johanson Technology
(b)	Stripline Al cantilever[9]: 5-300N PrimeNano			Quarter wave TL: FMBC002 Fairview Microwave, $l_{\mathrm{TL}} = 21$ mm
	5	0.5	1	$l_{\mathrm{stub}} = 24$ mm
(c)	Bare Pt cantilever: 25Pt400B Rocky Mountain Nanotechnology			$R_{\mathrm{shunt}} = 52$ Ω
	0.17	0.28	0.03	

that they can be modeled with lumped elements. The detailed simulation parameters are presented in Table I.

In all cases, we assume a coax transmission line (TL) with 50 Ω characteristic impedance delivering an input power of -20 dBm. We set the zero phase reference point to be the end of the TL, so $V_{\mathrm{in}} = 0.032\angle 0^{\circ}$ V. We simulate the reflection coefficient S_{11} looking into the impedance matching network (Fig. 2d) and the microwave voltage at the probe, V_{probe}, between 1.5 and 2.5 GHz (Fig. 2e). Without loss of generality, the total probe admittance Y_{probe} is then varied by $\Delta Y = (1-\mathrm{i}) \times 12.5$ nS to simulate a moderate variation of $\hat{\varepsilon}$ immediately under the tip (the imaginary part of ΔY corresponds to a capacitance change of ~ 1 aF at 2 GHz). The resulting change in the reflected microwave ΔV_{out} is then sampled at the same point as V_{in} and amplified by a total voltage gain of $G = 10^6$ to obtain the MIM signal ΔV_{MIM} (Fig. 2f).

Now we present our numerical results. Case (a) and (b) exhibit narrow-band impedance matching because only low-loss TLs and capacitors are used, while the shunt resistor in (c) exhibits broadband matching, as expected (Fig. 2d). The minimum $|S_{11}|$ exceeds -20 dB in all cases. For the probe voltage V_{probe}, while it has the same magnitude as V_{in} for the shunt resistor matching, it is amplified or suppressed within or outside the matched band for the two narrow-band matching schemes. The amplification is up to $\sim$10 and 4 (Fig. 2e) for case (a) and (b). We can understand this behavior by recognizing the narrow-band matching networks as microwave resonators of different quality factors (Q factors), and the lower Q factor in (b) is mainly due to the higher loss in the stripline probe.

The difference in V_{probe} is directly reflected in ΔV_{MIM} (Fig. 2f). For a fixed ΔY, case (c) has a small signal that is nearly constant in both amplitude and phase across a wide frequency range, while cases (a) and (b) have greatly enhanced signals in the matched band with sharp phase changes across the resonance, and suppressed signals outside the matched band. This agrees well with the empirical knowledge that low-loss probes and narrow-band matching networks give rise to higher signals but are more susceptible to environmental fluctuations.

Nevertheless, despite the distinct behaviors of the three cases, we found that the dimensionless quantity $(2\Delta V_{\mathrm{MIM}} V_{\mathrm{in}} Y_0)/(G V_{\mathrm{probe}}^2 \Delta Y) \approx -1$ across the entire simulated frequency range in all cases (Fig. 2g). With this numerical insight, we analytically derive the universal scaling relationship below.

The universal scaling arises from the linearity and reciprocity of our microwave circuits. At any given frequency, any two-port linear circuit can be described by its equivalent complex admittance matrix

$$\hat{Y} = \begin{bmatrix} Y_{11} & Y_{12} \\ Y_{21} & Y_{22} \end{bmatrix}.$$

If the circuit is reciprocal ($Y_{21} = Y_{12}$), it can be further described by a π-shaped admittance network[14]. All impedance matching networks used in MIM so far are linear and reciprocal, and can therefore be modeled as such, with port 1 connecting to the microwave reflectometer through a Y_0 transmission line[15] and port 2 connecting to the microwave probe that can be described by a complex admittance Y_{probe} based on the probe's lumped element values (Fig. 3).

The reflected microwave amplitude V_{out} is the product of the incident amplitude V_{in} and the complex reflection coefficient S_{11}:

$$V_{\mathrm{out}} = S_{11} V_{\mathrm{in}},$$

where

$$S_{11} = \frac{Y_0 - Y_{\mathrm{L}}}{Y_0 + Y_{\mathrm{L}}},$$

and Y_{L} is the total equivalent load admittance looking into port 1 of the impedance matching network

$$Y_{\mathrm{L}} = Y_{11} - \frac{Y_{12}^2}{Y_{22} + Y_{\mathrm{probe}}}.$$

Therefore, for a small change of ΔY in Y_{probe}, the corresponding change in V_{out} is

$$\begin{aligned} \Delta V_{\mathrm{out}} &= \Delta Y \frac{\partial V_{\mathrm{out}}}{\partial Y_{\mathrm{probe}}} = \Delta Y V_{\mathrm{in}} \frac{\partial S_{11}}{\partial Y_{\mathrm{L}}} \frac{\partial Y_{\mathrm{L}}}{\partial Y_{\mathrm{probe}}} \\ &= -2\Delta Y V_{\mathrm{in}} Y_0 \left[\frac{Y_{12}}{(Y_{22} + Y_{\mathrm{probe}})(Y_0 + Y_{11}) - Y_{12}^2}\right]^2. \end{aligned} \tag{1}$$

We can also solve for $V_{\mathrm{probe}} (= V_2)$ using standard voltage division and the fact that $V_1 = V_{\mathrm{in}} + V_{\mathrm{out}}$ to obtain

$$V_{\mathrm{probe}} = -\frac{2 Y_{12} V_{\mathrm{in}} Y_0}{(Y_{22} + Y_{\mathrm{probe}})(Y_0 + Y_{11}) - Y_{12}^2}.$$

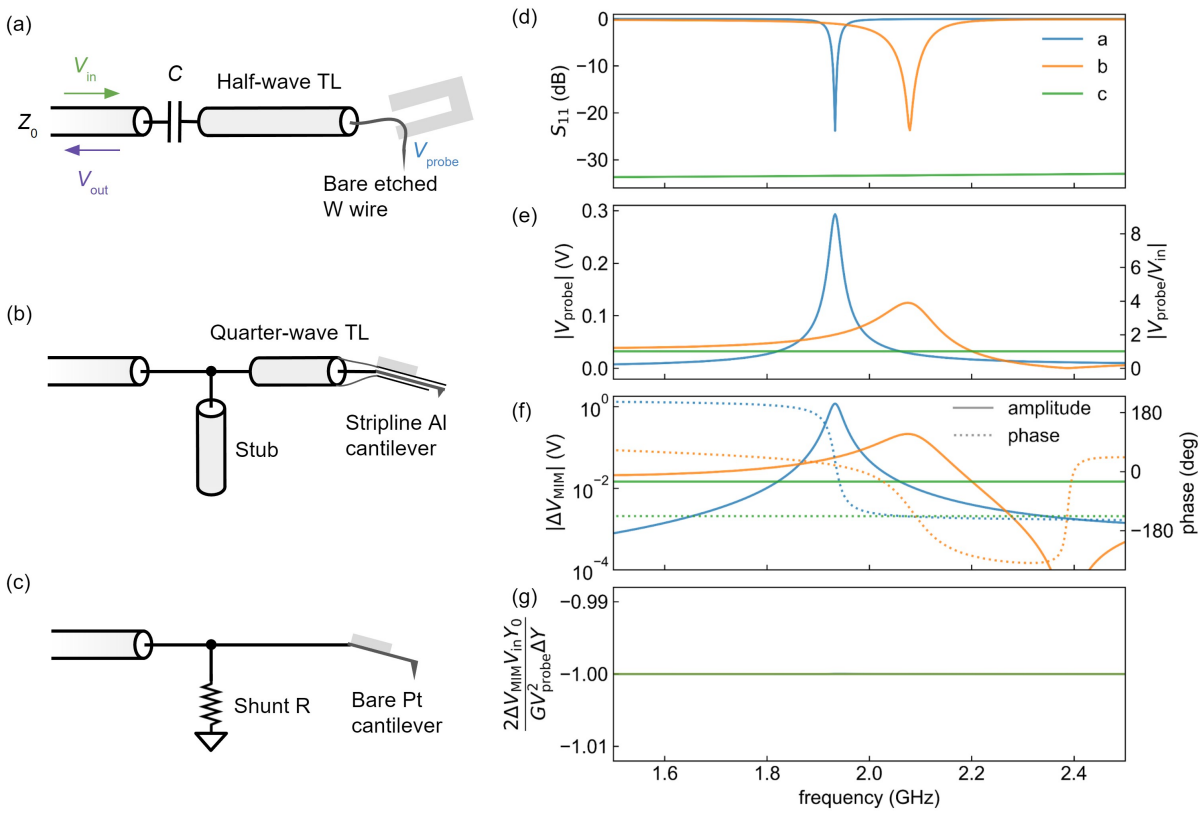

FIG. 2. (a)-(c) The schematics of three distinct combinations of microwave probes and impedance matching networks: (a) quartz tuning fork (TF) probe with half-wave matching, (b) stripline cantilever probe with quarter-wave and stub matching, and (c) bare metal cantilever probe with broadband shunt resistor matching. The gray shades represent the TF in (a) and the probe carrier chips in (b) and (c). (d) Simulated S_{11} looking into the impedance matching network between 1.5 GHz and 2.5 GHz for the three different cases. (e) Simulated quasi-static voltage at the probe, V_{probe}. The right axis shows values normalized by V_{in}. (f) Simulated MIM signal, ΔV_{MIM}. In practice, instead of amplitude and phase, it is often recorded as Re/Im$[\Delta V_{\text{MIM}}]$. (g) The dimensionless quantity $(2\Delta V_{\text{MIM}} V_{\text{in}} Y_0)/(G V_{\text{probe}}^2 \Delta Y)$.

We can thus define

$$\eta = \frac{V_{\text{probe}}}{V_{\text{in}}} = -\frac{2Y_{12}Y_0}{(Y_{22}+Y_{\text{probe}})(Y_0+Y_{11})-Y_{12}^2}. \tag{2}$$

η is a dimensionless factor that is determined by the circuit ($\hat{Y}$, Y_0, and Y_{probe}) but manifests in the ratio $V_{\text{probe}}/V_{\text{in}}$.

Combining Eq. (1) and (2), we obtain

$$\Delta V_{\text{out}} = -\frac{\Delta Y}{2Y_0}\eta^2 V_{\text{in}}.$$

ΔV_{out} is then amplified by a total voltage gain G to obtain the MIM signal

$$\Delta V_{\text{MIM}} = -G \cdot \frac{\Delta Y}{2Y_0} \cdot \eta^2 \cdot V_{\text{in}}. \tag{3}$$

Rearranging this equation yields $(2\Delta V_{\text{MIM}} V_{\text{in}} Y_0)/(G V_{\text{probe}}^2 \Delta Y) \approx -1$, consistent with the numerical result (Fig. 2g).

Next, we discuss the implications and corollaries of this result. First, we note that the derivation above can be carried out for any linear and reciprocal circuit at any frequency, so the relationship holds regardless of the type of matching network or probe, and can be extended to other microwave sensing and metrology techniques with similar circuits. It shows that the details of the matching network are completely encoded in $\eta = V_{\text{probe}}/V_{\text{in}}$, and thus we can attribute the gain or loss of sensitivity to the amplification or suppression of the voltage at the probe relative to the incident wave, with no additional

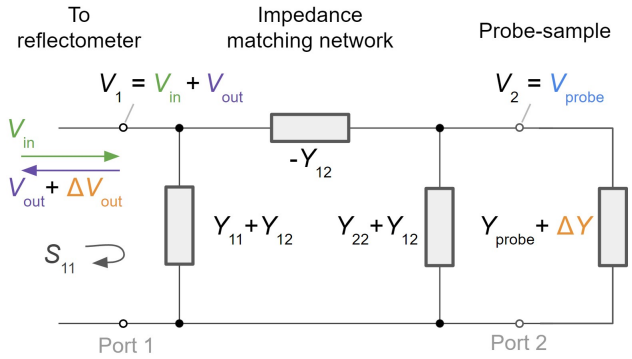

FIG. 3. Equivalent circuit diagram of an MIM matching-network-probe combination that is linear and reciprocal.

free design parameters other than G and Y_0. Conversely, one can calculate η by measuring $\hat{Y}$ and Y_{probe} separately and then using Eq. (2) to gain insight into the sensitivity.

Second, we can obtain the scaling law of maximum signal as a function of η for two distinct operation regimes. If the operation is limited by the maximum incident power $V_{\text{in;max}}$ due to limited cancellation power range or cross-talk within the microwave reflectometer, Eq. (3) straightforwardly shows that the maximum signal will scale with η^2:

$$\Delta V_{\text{MIM;max}} = -G \cdot \frac{\Delta Y}{2Y_0} \cdot \eta^2 \cdot V_{\text{in;max}}$$

Instead, if the operation is limited by the maximum probe voltage $V_{\text{probe;max}}$ due to sample perturbation, heating, or damage[16], we can rewrite Eq. (3) as

$$\Delta V_{\text{MIM}} = -G \cdot \frac{\Delta Y}{2Y_0} \cdot \eta \cdot V_{\text{probe}}$$

which shows that the maximum signal will scale linearly with η:

$$\Delta V_{\text{MIM;max}} = -G \cdot \frac{\Delta Y}{2Y_0} \cdot \eta \cdot V_{\text{probe;max}}$$

In both regimes, if the goal is to maximize signal in a narrow band, one should maximize η by minimizing loss in the matching-network-probe combination with, e.g., superconducting components. The sharpness of the resonance will, however, increase the sensitivity to source phase noise and environmental fluctuations (Fig. 2f).

Third, we note that better impedance matching does not necessarily lead to higher sensitivity. For example, replacing the TLs in case (a) with lower-loss models lead to significantly worse impedance matching but significantly higher sensitivity (Fig. 4). Therefore, the quality of the impedance matching is not a sufficient indicator of MIM performance on its own.

Fourth, our result presents a potentially viable path for using broadband resistive matching for microwave impedance nano-spectroscopy or hyper-spectral imaging. A shunt resistor matching has $\eta \sim 1$ and a typical narrow-band matching has $\eta \lesssim 10$. Therefore, in the sample perturbation limit ($V_{\text{probe}} = V_{\text{probe;max}}$) where the maximum signal scales linearly with η, the signal is only reduced by a factor of $\lesssim 10$ if switched from a narrow-band to a broadband resistive matching. The reduction in signal-to-noise ratio (SNR) is likely even less thanks to the reduced sensitivity to environmental fluctuations and source phase noise. Such a moderate reduction in SNR may be compensated by, e.g., increasing the tip apex diameter by a factor of ~ 3 to increase ΔY, which may be a worthy compromise for gaining the ability to perform broadband, continuously-tunable-frequency local spectroscopy. That being said, in the incident power limited regime, the signal reduction of η^2 is likely too great to be manageable.

Finally, the maximum signal scaling and the sensitivity-bandwidth trade-off from our result only apply to linear and reciprocal matching-network-probe combinations. Therefore, leveraging nonlinear components, nonreciprocal media, or active devices can potentially go beyond these limits in a new generation of MIM and other similar microwave sensing and metrology techniques.

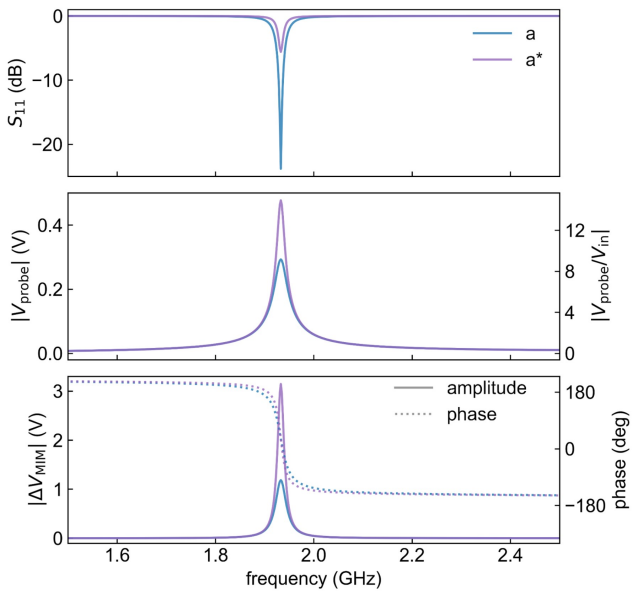

FIG. 4. Better impedance matching does not necessarily lead to higher sensitivity. Case (a) is the same as that in Fig. 2; case (a*) is the same as (a) except that a lower loss transmission line (Fairview FMBC008) is used. Around 2 GHz, the attenuation of case (a) is approximately 1 dB/m, while the attenuation of case (a*) is approximately 0.3 dB/m. Case (a*) has significantly worse impedance matching but significantly higher sensitivity.

ACKNOWLEDGMENTS

We thank Nathaniel Morrison for helpful feedback on our manuscript. This work was supported by the Laboratory Directed Research and Development Program of Lawrence Berkeley National Laboratory under U.S. Department of Energy Contract No. DE-AC02-05CH11231.

DATA AVAILABILITY

The data that support the findings of this study are available from the corresponding author upon reasonable request.

REFERENCES

[1] K. Lai, M. B. Ji, N. Leindecker, M. A. Kelly, and Z. X. Shen, "Atomic-force-microscope-compatible near-field scanning microwave microscope with separated excitation and sensing probes," Rev. Sci. Instrum. **78**, 063702 (2007).

[2] M. E. Barber, E. Y. Ma, and Z.-X. Shen, "Microwave impedance microscopy and its application to quantum materials," Nat. Rev. Phys. **4**, 61–74 (2022).

[3]Z. Chu, C.-Y. Wang, J. Quan, C. Zhang, C. Lei, A. Han, X. Ma, H.-L. Tang, D. Abeysinghe, M. Staab, X. Zhang, A. H. MacDonald, V. Tung, X. Li, C.-K. Shih, and K. Lai, "Unveiling defect-mediated carrier dynamics in monolayer semiconductors by spatiotemporal microwave imaging," Proc. Natl. Acad. Sci. U.S.A. **117**, 13908–13913 (2020).

[4]L. Zheng, H. Dong, X. Wu, Y.-L. Huang, W. Wang, W. Wu, Z. Wang, and K. Lai, "Interferometric imaging of nonlocal electromechanical power transduction in ferroelectric domains," Proc. Natl. Acad. Sci. U.S.A. **115**, 5338–5342 (2018).

[5]E. Y. Ma, Y.-T. Cui, K. Ueda, S. Tang, K. Chen, N. Tamura, P. M. Wu, J. Fujioka, Y. Tokura, and Z.-X. Shen, "Mobile metallic domain walls in an all-in-all-out magnetic insulator," Science **350**, 538–541 (2015).

[6]Y. Shi, J. Kahn, B. Niu, Z. Fei, B. Sun, X. Cai, B. A. Francisco, D. Wu, Z.-X. Shen, X. Xu, D. H. Cobden, and Y.-T. Cui, "Imaging quantum spin Hall edges in monolayer WTe2," Sci. Adv. **5**, eaat8799 (2019).

[7]E. Y. Ma, M. R. Calvo, J. Wang, B. Lian, M. Mühlbauer, C. Brüne, Y.-T. Cui, K. Lai, W. Kundhikanjana, Y. Yang, *et al.*, "Unexpected edge conduction in mercury telluride quantum wells under broken time-reversal symmetry," Nat. Commun. **6**, 1–6 (2015).

[8]K. Lai, W. Kundhikanjana, M. A. Kelly, and Z.-X. Shen, "Nanoscale microwave microscopy using shielded cantilever probes," Appl. Nanosci. **1**, 13–18 (2011).

[9]Y. Yang, K. Lai, Q. Tang, W. Kundhikanjana, M. A. Kelly, K. Zhang, Z.-x. Shen, and X. Li, "Batch-fabricated cantilever probes with electrical shielding for nanoscale dielectric and conductivity imaging," J. Micromech. Microeng. **22**, 115040 (2012).

[10]Y. Yang, E. Y. Ma, Y.-T. Cui, A. Haemmerli, K. Lai, W. Kundhikanjana, N. Harjee, B. L. Pruitt, M. Kelly, and Z.-X. Shen, "Shielded piezoresistive cantilever probes for nanoscale topography and electrical imaging," J. Micromech. Microeng. **24**, 045026 (2014).

[11]Y.-T. Cui, E. Y. Ma, and Z.-X. Shen, "Quartz tuning fork based microwave impedance microscopy," Rev. Sci. Instrum. **87**, 063711 (2016).

[12]S. R. Johnston, E. Y. Ma, and Z.-X. Shen, "Optically coupled methods for microwave impedance microscopy," Rev. Sci. Instrum. **89**, 043703 (2018).

[13]D. Lee, Q. Liu, L. Zheng, X. Ma, H. Li, M. Li, and K. Lai, "Direct Visualization of Gigahertz Acoustic Wave Propagation in Suspended Phononic Circuits," Phys. Rev. Appl. **16**, 034047 (2021).

[14]D. M. Pozar, *Microwave Engineering*, 4th ed. (Wiley, Hoboken, NJ, 2011).

[15]Including the transmission line between the reflectometer and the impedance matching network as part of the network itself changes the numerical values in $\hat{Y}$ but does not change the derivation.

[16]Here we assume that the probe itself is sufficiently low-loss such that the voltage at the connection point V_{probe} is very close to that at the tip apex V_{tip}.